

Article

Control Optimization of Solar Thermally Driven Chillers

Antoine Dalibard *, Daniel Gürlich, Dietrich Schneider and Ursula Eicker

Research Center of Sustainable Energy Technology, Stuttgart University of Applied Sciences, Schellingstr. 24, 70174 Stuttgart, Germany; daniel.guerlich@hft-stuttgart.de (D.G.); dietrich.schneider@hft-stuttgart.de (D.S.); ursula.eicker@hft-stuttgart.de (U.E.)

* Correspondence: antoine.dalibard@hft-stuttgart.de; Tel.: +49-711-8926-2981

Academic Editor: Francesco Calise

Received: 3 August 2016; Accepted: 13 October 2016; Published: 25 October 2016

Abstract: Many installed solar thermally driven cooling systems suffer from high auxiliary electric energy consumption which makes them not more efficient than conventional compression cooling systems. A main reason for this is the use of non-efficient controls with constant set points that do not allow a chiller power modulation at partial-load and therefore lead to unnecessary high power consumption of the parasitics. The aims of this paper are to present a method to control efficiently solar thermally driven chillers, to demonstrate experimentally its applicability and to quantify the benefits. It has been shown that the cooling capacity of a diffusion absorption chiller can be modulated very effectively by adjusting both the temperature and the flow rate of the cooling water. With the developed approach and the use of optimization algorithms, both the temperature and the flow rate can be controlled simultaneously in a way that the cooling load is matched and the electricity consumption is minimized. Depending on the weather and operating conditions, electricity savings between 20% and 60% can be achieved compared to other tested control approaches. The highest savings are obtained when the chiller is operated at partial load. The presented method is not restricted to solar cooling systems and can also be applied to other conventional heating ventilation and air conditioning (HVAC) systems.

Keywords: control strategy; solar cooling; heat rejection; optimization; absorption chiller

1. Introduction

Refrigeration and air conditioning of buildings are responsible for about 17% of worldwide electricity consumption [1]. This demand is expected to increase significantly over the next several decades [2,3]. The main reasons for this development are an increased living standard, a growing population in hot climates, higher internal loads, recent architectural trends with more glass in the building envelope, and, last but not least, the rising temperatures induced by anthropogenic climate change. Therefore, it is a far-sighted decision to cover this cooling energy demand with energy efficient and low-carbon technologies avoiding future reinforcement of anthropogenic climate change. The European Union addresses these issues with binding legislations like the “2030 climate and energy framework” [4] from 2014 and the “EUROPE 2020” strategy from the year 2010. The first one aims to a 40% reduction of the greenhouse gas emissions (from 1990 levels) until the year 2030, a share of 24% for renewable energy and an increase in energy efficiency of about 27%. In this regard, efficiency measures are crucial in the building cooling sector in order to achieve these ambitious objectives.

Solar thermal cooling systems (STCS) are an interesting option for the cooling of buildings under many boundary conditions and should always be considered as an alternative in the planning phase of a building project [5–7]. In contrast to compression chillers, thermally driven chillers (TDC)

have low internal electricity consumption since they do not use electrically driven compressors. Absorption chillers use a small pump to circulate the solution internally, whereas TDC using water as refrigerant (LiBr/water absorption and adsorption chillers) may require a vacuum pump periodically. Diffusion absorption chillers do not have any power requirement since the solution pump is driven thermally. However, detailed monitoring data showed that the overall electrical efficiency of many existing STCS (including all components) is much lower than expected, not necessarily above that of conventional compression systems [8]. The reasons for this poor performance are various and can be different from one system to another. The most frequently cited reason is a lack of control. The speed of circulating pumps and fans are commonly kept constant, which provides no possibility to adapt the chiller cooling capacity to the building cooling load and leads to an unnecessary high power consumption of the auxiliaries (pumps, fans, etc.) [8]. Therefore, it is required to develop innovative control strategies that allow a chiller power modulation with a minimum power consumption of the parasitics [9].

The majority of installed STCS use on/off or fixed set-points controls to operate the system components in a way to provide as much cold as possible without consideration to the cooling demand and the power consumption of the parasitics. In this regard, more advanced concepts have been investigated by several authors within the past 10 years. The concept of critical radiation has been used by Bujedo et al. to control the solar pump of a solar absorption chiller driven system [10]. This control leads to an increase of 8% in solar yield but does not allow for adjustment of the chiller driving temperature according to the demand. Another approach is to control the hot water temperature in a way to maximise the solar coefficient of performance (COP) defined as the ratio of useful cold produced to the incoming solar radiation on the collectors [11]. Following this idea, Lecuona et al. showed that this temperature can be calculated and fed into the controller by using equations that describe the part-load behaviour of the chiller and the collectors, respectively [12]. A drawback of this approach is that the cooling capacity of the chiller cannot be controlled and the goal of this control does not ensure a good system overall performance. Instead of adjusting the hot water temperature, the cooling water temperature can be controlled in order to modulate the cooling capacity of an absorption chiller according to the cooling demand [13]. A modified version of the characteristic equation of sorption chillers [14] can be used to predict the part-load performance of the absorption chiller. Significant electricity savings are theoretically possible by using this approach (up to 50% compared to constant full speed cooling tower fan operation).

If, to achieve a given control goal, the variables to be controlled are greater than one, an optimization procedure might be necessary to compute the required set-points. Sonntag et al. implemented such supervisory control in a solar air conditioning plant. The control goal was to match the cooling demand and at the same time minimize the gas heater contribution to the absorption chiller heat input. The authors mentioned the importance of having good models of the main system components for the robustness of such control [15]. Another approach consists in controlling both hot and cooling water together in order to minimize the specific cost of produced cold for a given cooling capacity. Again, a modified characteristic equation is used to describe the part-load behavior of the adsorption chiller and two additional equations are needed for the description of both thermal and electrical performance of the cooling tower. Some simplifications are made in order to reduce the complexity of the cost function and solve the minimization problem without using a specific optimization algorithm [16]. This control approach has been implemented in a large solar thermal cooling plant. However, the monitoring results showed a poor global electrical performance since this aspect is not considered in the cost function to be optimized [17]. Using a similar approach, the cooling power of an adsorption chiller can be adjusted according to the cooling demand by controlling simultaneously hot and cooling water temperatures together with the chiller cycle time [18]. An optimization algorithm is used within the controller to calculate the set points that minimize the system electricity consumption. According to the simulation results, this strategy allows significant

primary energy savings compared to conventional control strategies (without variable set point controls). However, the robustness of such algorithms in real controllers still needs to be proven.

In this paper, based on the mentioned works, a method that allows for controlling the cooling capacity of the thermally driven chiller, and, at the same time, minimizing the electricity consumption is presented. Since the heat rejection is responsible for more than 60% of the total electricity consumption, this paper will focus on the control of the cooling water pump and the cooling tower fan [19]. The method is then applied in an experimental set-up to control a small scale diffusion absorption chiller coupled with an open wet cooling tower. Depending on the ambient conditions (weather and temperatures), electricity savings between 20% and 60% can be achieved compared to other tested control approaches.

2. Methodology

2.1. Control Approach

Figure 1 shows a simplified hydraulic scheme of a solar thermal cooling plant with the main energy flows and the nomenclature that will be used in this work. The main component of such systems is the TDC since it provides the cold to the building. The cooling capacity of the chiller \dot{Q}_{LT} can be influenced by acting on the operating conditions of temperature and flow rates at the three temperature levels: high temperature HT , middle temperature MT and low temperature LT . The hot water temperature T_{HT} is mainly determined by the available solar irradiation but can be influenced by controlling the solar pumps and/or by using a mixing valve between the hot storage and the chiller [9]. The chilled water temperature T_{LT} is usually fixed in a certain range by the cooling distribution system of the building. The heat rejection or cooling water temperature T_{MT} can be controlled by adjusting the speed of the cooling tower fan and/or the cooling water pump. The minimum achievable heat rejection temperature is the ambient temperature T_{amb} if dry coolers are used and the wet bulb temperature T_{wb} in case of wet cooling towers.

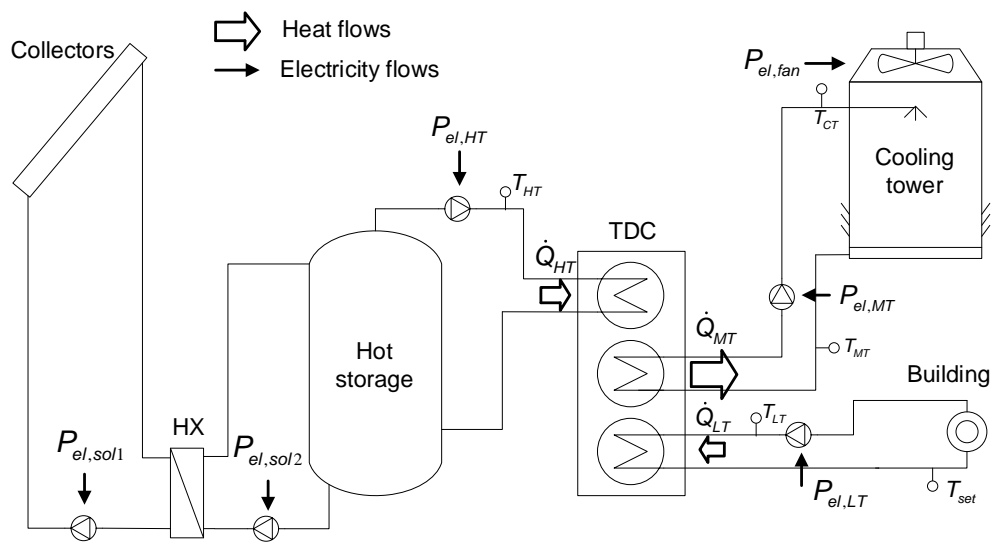


Figure 1. Simplified scheme of a solar thermal cooling plant with the main energy flows.

The present work focuses on the control of the heat rejection since it is the highest power consumer. Consequently, only the control of the cooling water flow rate and the temperature is considered. As mentioned previously, a major drawback of conventional control strategies is the lack of control of the chiller's cooling capacity. Therefore, the main goal of the control strategies developed in this paper is to adjust the chiller cooling capacity \dot{Q}_{LT} to the building cooling load, i.e. to provide chilled water

at a given set temperature T_{set} . The required cooling capacity $\dot{Q}_{LT,req}$ can be calculated according to Equation (1) if the flow rate \dot{V}_{LT} and the temperature T_{LT} of the chilled water are known (measured):

$$\dot{Q}_{LT,req} = \rho_{LT} \cdot \dot{V}_{LT} \cdot c_{p,LT} \cdot (T_{LT} - T_{set}) \quad (1)$$

In the following, three different control strategies able to fulfill that goal (Equation (1)) are proposed. This paper does not focus on the ON/OFF operation of the main components but on the optimisation of the main controlled parameters (temperature and flow rate) of the heat rejection loop during operation.

2.2. Investigated Control Strategies

The volumetric flow rates of the hot and chilled water \dot{V}_{HT} and \dot{V}_{LT} are constant for all described control strategies.

2.2.1. Mode 1

The cooling water flow rate \dot{V}_{MT} is kept constant. The cooling water temperature T_{MT} is controlled by adjusting the cooling tower fan speed (proportional integral (PI) controller) in a way that the cooling load is matched (Equation (1)). An additional equation that expresses the cooling capacity of the chiller (at steady state) in the functioning of the main operating conditions of temperatures and flow rates is needed to calculate the cooling water temperature set point dynamically (Equation (2)):

$$\dot{Q}_{LT} = f(T_{HT}, T_{MT}, T_{LT}, \dot{V}_{MT}) \quad (2)$$

Equation (2) might be of a different nature: an expression with a physical meaning like the characteristic equation of sorption chillers [14] or any kind of correlation. Within this work, a polynomial expression has been fitted with measurement data using the least square method (see Section 3.2 and Appendix B). The required cooling water temperature set point that allows the chiller to meet the cooling demand is derived from Equations (1) and (2). Depending on the complexity of Equation (2), an iteration process is needed or not.

2.2.2. Mode 2

The cooling tower fan speed is controlled (PI controller) to provide a constant cooling water temperature to the chiller. The cooling water flow rate is controlled by adjusting the pump speed (PI controller) in a way that the cooling demand is matched. Again, the required flow rate is calculated from Equations (1) and (2).

2.2.3. Mode 3

In this mode, both cooling water temperature and flow rate are simultaneously controlled in a way that the cooling load is matched (Equation (1) fulfilled) and at the same time that the total power consumption is minimised (Equation (3)).

$$P_{el,tot} = \sum P_{el,x} \quad (3)$$

The principle of this control strategy is illustrated in Figure 2. At given operating conditions (temperatures and flow rate of hot and chilled water) and ambient conditions (wet bulb temperature), the actual cooling load can be matched in a way that the total system power consumption is minimised by adjusting both the cooling tower fan and pump speed. The duty of the controller algorithm is to find this optimum point. The flow chart of the algorithm used to find the optimum is shown in Appendix A.

In order to do so, additional equations that describe the part-load behavior of both the chiller and the cooling tower (Equations (4)–(6)) as well as the relationship of the pump and fan speed to the power consumption are required (Equations (7) and (8)):

$$\dot{Q}_{HT} = g(T_{HT}, T_{MT}, T_{LT}, \dot{V}_{MT}) \quad (4)$$

$$\dot{Q}_{MT} = \dot{Q}_{HT} + \dot{Q}_{LT} \quad (5)$$

$$\dot{Q}_{MT} = h(T_{CT}, \dot{V}_{MT}, T_{wb}, f_{fan}) \quad (6)$$

$$P_{el, fan} = f_1(f_{fan}) \quad (7)$$

$$P_{el, MT} = f_2(f_{pump}) \quad (8)$$

The thermal power of the heat rejection unit \dot{Q}_{MT} depends on the temperature entering the cooling tower T_{CT} and the flow rate of the cooling water \dot{V}_{MT} , on the wet bulb temperature T_{wb} (for wet cooling towers) and on the fan frequency f_{fan} . Again, different kinds of models can be used. In this work, polynomial expressions have been fitted with measurement data using the least square method (see Section 3.2 and Appendix B). Both cooling water set points (temperature and flow rate) are determined by using Equations (1)–(8) in an optimization procedure so that Equation (1) is fulfilled and Equation (3) is minimized.

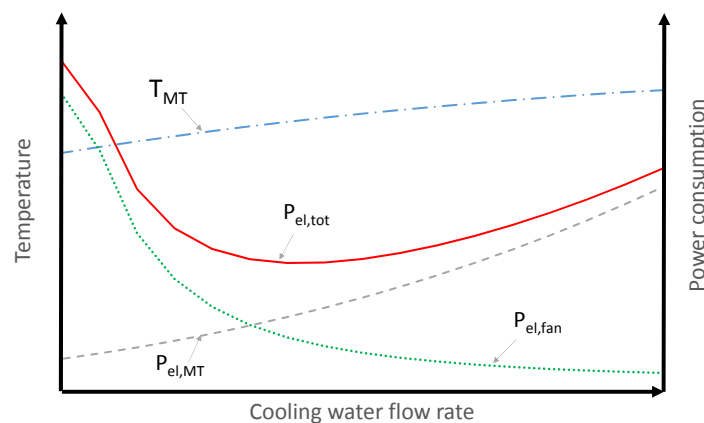


Figure 2. Principle of heat rejection control optimization mode 3 (at given $\dot{Q}_{LT, req}$, T_{HT} , T_{LT} , T_{wb} , \dot{V}_{HT} and \dot{V}_{LT}).

2.2.4. Overview

Table 1 gives an overview of the three control strategies.

Table 1. Overview of the investigated control strategies.

| Mode | Variable Set Point | Control Parameter | Objective(s) |
|------|---------------------------|--------------------|-------------------------------------|
| 1 | T_{MT} | Fan speed | Cover load |
| 2 | \dot{V}_{MT} | Pump speed | Cover load |
| 3 | T_{MT} & \dot{V}_{MT} | Fan and pump speed | Cover load & Minimize $P_{el, tot}$ |

2.3. Performance Indicators

The overall system efficiency at a given instant t is given by the energy efficiency ratio (EER), which is defined as the ratio of the chiller cooling capacity \dot{Q}_{LT} to the actual system power consumption (Equation (9)). The system efficiency over a period of time $\Delta t = t_1 - t_0$ is called average energy

efficiency ratio (AEER) and is obtained by integrating the EER over the time (This indicator would be the daily equivalent of the so-called Seasonal Energy Efficiency Ratio (SEER)). These performance indicators will be used to compare the investigated control strategies:

$$EER(t) = \frac{\dot{Q}_{LT}(t)}{P_{el,tot}(t)} = \frac{\dot{Q}_{LT}(t)}{\sum P_{el,x}(t)} \quad (9)$$

$$AEER(t_0, t_1) = \int_{t_0}^{t_1} EER(t) dt = \frac{\int_{t_0}^{t_1} \dot{Q}_{LT}(t) dt}{\int_{t_0}^{t_1} P_{el,tot}(t) dt} \quad (10)$$

3. Experimental Set-Up

3.1. Description

3.1.1. Hardware Components

The main hardware components of the experimental set-up are shown schematically in Figure 3. The central component is a diffusion ammonia/water absorption chiller as the last version of several prototypes developed at the Stuttgart University of Applied Sciences [20]. The particularity of such technology is that the chillers do not need electricity to run the refrigerant cycle internally. The internal circulation of the solution is realized with a thermally driven pump also called bubble pump and the refrigerant is circulated through buoyancy effects. The designed cooling capacity is 5 kW_{th} , but, for this work, the internal pressure and the solution concentration have been modified in order to operate the chiller with lower driving temperatures and higher heat rejection temperatures. With these modifications, the maximal cooling capacity is lower (around 3.8 kW_{th} at $T_{HT} = 95 \text{ }^\circ\text{C}$, $T_{MT} = 20 \text{ }^\circ\text{C}$ and $T_{LT} = 18 \text{ }^\circ\text{C}$). The heat rejection is performed with a large open wet cooling tower of 40 kW_{th} maximum heat rejection capacity (for $T_{CT} = 27 \text{ }^\circ\text{C}$ and $T_{wb} = 21 \text{ }^\circ\text{C}$) and 0.43 kW_{el} fan maximal power consumption. The cooling water pump (P_{MT}) has been oversized (1.5 kW_{el}) to compensate the high pressure drops of the laboratory hydraulics, which are due to monitoring and investigation purposes and are unnecessary in the case of real systems. For this work, the maximum pump power consumption has been reduced to 0.4 kW_{el} , thus it is more conform to typical values for such a system size [21]. The cooling water coming from the cooling tower flows first into the condenser and then in the absorber (serie configuration). At the outlet of the absorber, a part of the cooling water can be sent to the dephlegmator via a diverter valve. This valve is controlled in a way to provide a constant temperature of the ammonia vapour entering the condenser ($50 \text{ }^\circ\text{C}$). The solar system and the building cooling load are simulated with two electrical heaters (with integrated pumps) of 24 and 6 kW_{el} maximal heating capacity, respectively. Both electrical heaters use internal PI controllers to adjust their respective temperature set-points. The daily profiles used for the measurement are detailed in Section 3.3.

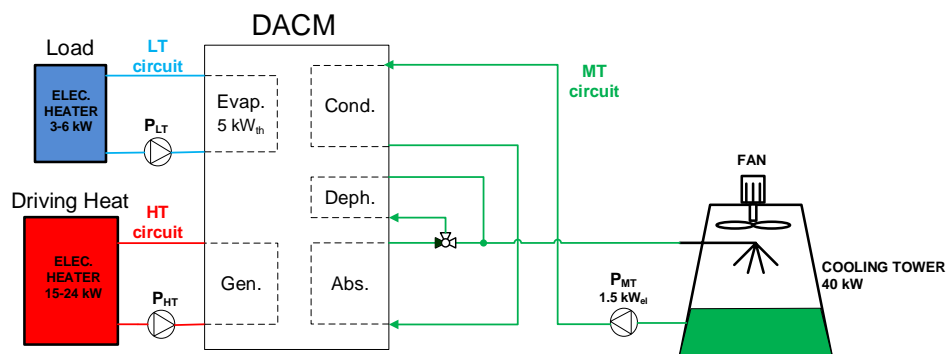


Figure 3. Simplified hydraulic scheme of the experimental set-up.

3.1.2. Measurement Devices

The temperatures of the three external circuits are measured with 4-wires PT100 sensors (1/3 DIN Class B) at the inlet and outlet of all the main components. The volumetric flow rates are measured with magnetic inductive (MID) flow meters and the ambient air conditions with a combined temperature and humidity sensor. The power consumption of the cooling water pump and cooling tower fan are measured with electricity meters. The accuracy of the measurement devices are shown in Table 2.

Table 2. Measurement equipment involved in the experiment.

| Measurement Device | Type | Accuracy |
|----------------------------|---------------------|--------------------|
| Flow meter | MID | 0.2% |
| Temperature sensors | PT100 (1/3 class B) | 0.1 + 0.0017·T |
| Humidity sensor | Capacitive | 2% (rel. humidity) |
| Ambient temperature sensor | PT100 | 0.2 K |
| Electricity meter | Electronic | 0.5% |

When a quantity Y is obtained from calculations involving measured data (x_1, x_2, \dots) , the uncertainty of this quantity U_Y is estimated assuming that individual measurement are uncorrelated and random by using a Gaussian distribution (Equation (11)):

$$U_Y = \sqrt{\sum_k \left(\frac{\partial Y}{\partial x_k} \right)^2 \cdot U_{x_k}^2} \quad (11)$$

3.1.3. Data Acquisition and Control

The data acquisition of the measured data was realized every 10 s with a data logger Agilent 34970A (Agilent Technologies, Inc., Santa Clara, USA). The visualization and the control have been done using Labview version 2010 (National Instruments Corporation, Austin, Texas, USA). The algorithms of the investigated control strategies have been programmed in Fortran and called from Labview. The speeds of the cooling water pump and cooling tower fan were PI controlled by the means of two frequency inverters piloted with a real-time controller cRIO-9024 (National Instruments Corporation, Austin, Texas, USA) coupled with Labview.

3.2. Characterization of the Main Components

The absorption chiller and the cooling tower have been tested under different operation conditions (of temperatures and flow rates) in order to elaborate a steady state performance map of the respective components. The operation variables like temperatures and volume flows have been measured and the corresponding values of the thermal powers \dot{Q}_x have been calculated using the following formula: $\dot{Q}_x = \rho_x \cdot \dot{V}_x \cdot c_{p,x} \cdot \Delta T_x$. The validity range of these performance maps as well as the steps used for the characterization are shown in Table 3. The steady state was assumed when the observed temperature changes at components outlet was less than 0.1 K (usually after about 10 min). From the measured performance maps, the characteristics equations that describe the part-load behaviour of both the chiller (\dot{Q}_{LT} and \dot{Q}_{HT}) and the cooling tower (\dot{Q}_{MT}) have been fitted. The mathematical form of these equations as well as the quality of the obtained fits are detailed in the Appendix B. In addition, second-degree polynomial functions have been derived to express the power consumption of the fan and the pump in function of the frequency speed (as shown in Equations (7) and (8)).

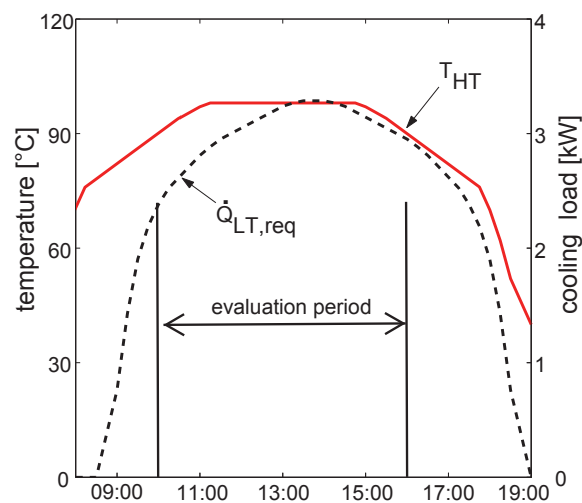
Table 3. Validity range of the chiller and cooling tower performance maps.

| Variable | DACM | Cooling Tower | Unit | Step |
|----------------|---------|---------------|----------------------------------|--|
| T_{HT} | 90–115 | - | °C | 5 K |
| T_{MT} | 20–28 | - | °C | 3 K |
| T_{LT} | 18 | - | °C | - |
| \dot{V}_{HT} | 2.9 | - | $\text{m}^3 \cdot \text{h}^{-1}$ | - |
| \dot{V}_{MT} | 1.8–3.6 | 1.8–3.6 | $\text{m}^3 \cdot \text{h}^{-1}$ | $0.45 \text{ m}^3 \cdot \text{h}^{-1}$ |
| \dot{V}_{LT} | 0.72 | - | $\text{m}^3 \cdot \text{h}^{-1}$ | - |
| T_{CT} | - | 20–36 | °C | 5 K |
| T_{wb} | - | 7–23.5 | °C | 3 K |
| f_{fan} | - | 50–100 | Hz | - |

DACM: Diffusion Absorption Cooling Machine, T_{HT} : Chiller inlet hot water temperature, T_{MT} : Chiller inlet cooling water temperature, T_{LT} : Chiller inlet chilled water temperature, \dot{V}_{HT} : Hot water flow rate, \dot{V}_{MT} : Cooling water flow rate, \dot{V}_{LT} : Chilled water flow rate, T_{CT} : Cooling water temperature at the inlet of the cooling tower, T_{wb} : Wet bulb temperature, f_{fan} : Cooling tower fan rotational frequency.

3.3. Investigated Daily Profile

In order to compare the different control strategies, a daily profile of irradiation (in the form of the hot water temperature) and building load has been fixed as shown in Figure 4. The defined hot water temperature T_{HT} profile corresponds to the output of about 25 m² of efficient solar thermal collectors (coupled with a 500 litres hot water storage) during a clear sunny day. This temperature has been limited to 100 °C since, above this temperature, the performance of the chiller (with this solution concentration and this internal pressure) decreases significantly. In practice, this temperature adjustment can be realized by the means of a mixing valve. This temperature has been used as set-point for the first electrical heater. In addition, a typical building load of an office building has been defined with a maximal cooling capacity of 3.2 kW_{th} and a constant return temperature of 18 °C (set-point used for the second electrical heater). The different control strategies have been tested for this defined profile under different ambient conditions of humidity and temperatures. Only the period between 10:00 and 16:00 has been evaluated since the bubble pump of the diffusion absorption chiller works only above 90 °C, which can be provided during a sunny day by the defined solar thermal plant when the irradiance reaches about 700 W·m⁻². An additional power consumption of 0.23 kW_{el} is added to the measured electricity in order to account for the additional pumps which are not included in the experimental set-up (solar and hot water pumps).

**Figure 4.** Hot water temperature and cooling load profile.

4. Results

4.1. Experiments

Figure 5 shows, by way of example, the daily measurement results of the three control strategies with comparable ambient conditions ($T_{wb} = 19\text{--}21\text{ }^{\circ}\text{C}$). The plots on the left-hand side show the measured ambient temperature T_{amb} , wet bulb temperature T_{wb} , inlet cooling water temperature to the chiller T_{MT} and the measured cooling water flow rate \dot{V}_{MT} . The plots on the right-hand side show the power consumption of both the fan $P_{el,fan}$ and the pump $P_{el,pump}$ as well as the chiller cooling capacity \dot{Q}_{LT} .

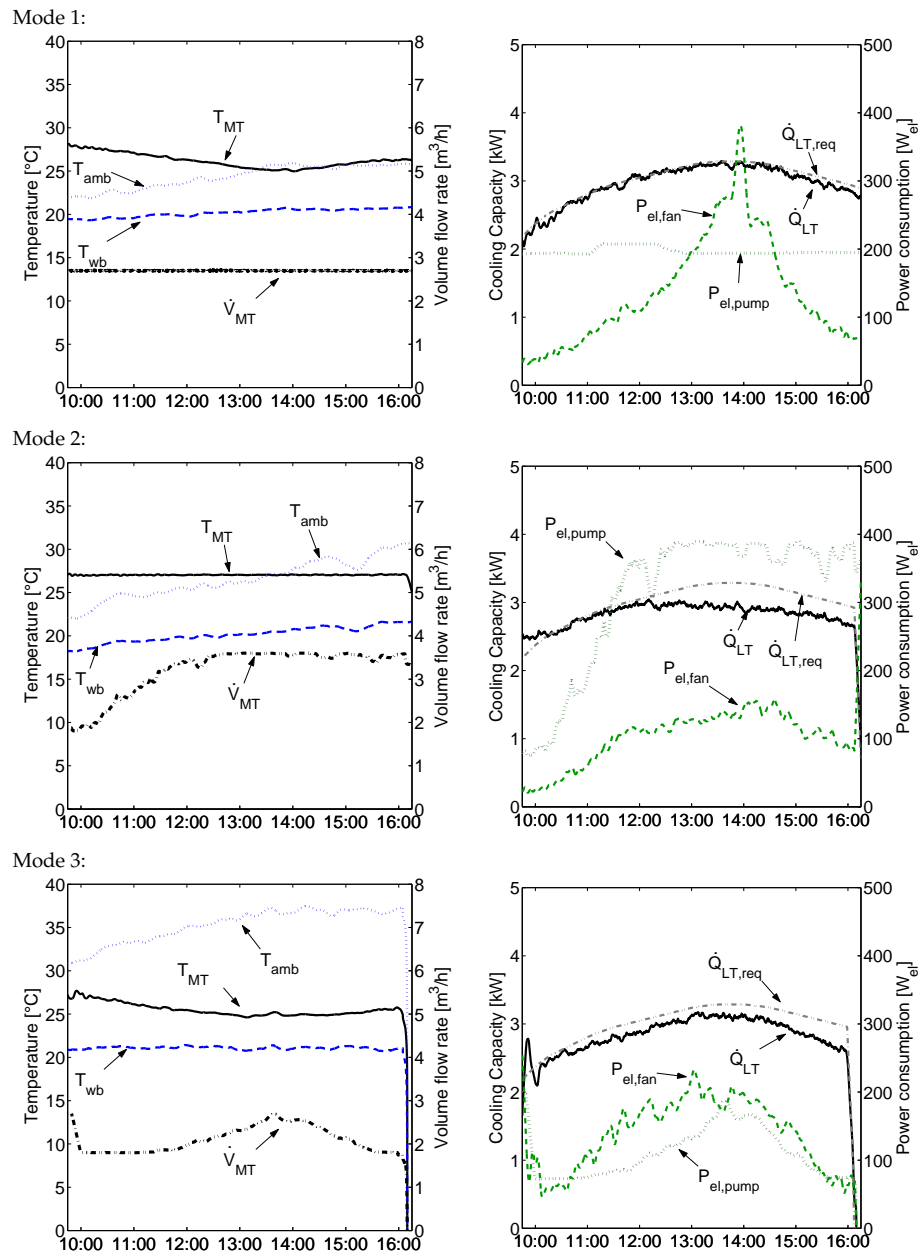


Figure 5. Results of the three control strategies on different days with comparable conditions (T_{wb} around $19\text{--}21\text{ }^{\circ}\text{C}$). On the left side, the ambient conditions (T_{amb} and T_{wb}) and the set point variables T_{MT} and \dot{V}_{MT} of the heat rejection circuit are drawn. The plots on the right side show the measured electrical consumptions ($P_{el,fan}$ and $P_{el,pump}$), the virtual cooling load $\dot{Q}_{LT,req}$ and actual chilled cooling capacity \dot{Q}_{LT} .

In mode 1 (two top plots in Figure 5), the cooling water is kept constant to around $2.7 \text{ m}^3 \cdot \text{h}^{-1}$ and the cooling water temperature is controlled in order to match the cooling load. At around 10:00, this temperature is set to around $28 \text{ }^\circ\text{C}$ so that the chiller can provide the 2.2 kW necessary. This temperature is then reduced progressively to $25 \text{ }^\circ\text{C}$ (by increasing the cooling tower fan speed) until the cooling load reaches its maximum (at 14:00) and is then again increased when the cooling load decreases. With this strategy, the cooling load can be matched very nicely during the whole day (at least in the case of the investigated chiller).

In the case of mode 2 (two plots in the middle in Figure 5), the cooling water temperature set-point is fixed to $27 \text{ }^\circ\text{C}$ and the flow rate is controlled in a way to match the cooling load. The flow rate is set to its minimum ($1.8 \text{ m}^3 \cdot \text{h}^{-1}$) at the beginning of the day (10:00) and is increased progressively with the rising cooling load. At around 12:30, the flow rate is set to its maximum so that the chiller cannot further meet the demand. This strategy suffers a lack of chiller power modulation for the allowed flow rate modulation range (and the investigated chiller).

For mode 3 (two plots below in Figure 5), both flow rate and temperature are controlled simultaneously in a way to match the load and to minimize the system power consumption. Both pump and fan are operated at reduced speed at the beginning of the day and are increased (or reduced) progressively in order to cope with the increasing (or reducing) cooling demand. It can be seen that the chiller did not fully match the cooling load. This can be explained by the fact that, on this specific day, the chiller start (before 10:00) did not happen as expected. The bubble pump of the chiller collapsed during the starting phase so that higher driving temperatures have been applied to the chiller in order to keep it running. As a result, the internal chiller pressure increased and the behaviour of the chiller was slightly different as measured during the characterization. This shows the importance of the characteristic equations in such a controlled approach. Other measurements show that this problem does not occur with a normal starting phase (see Appendix C). Despite the mentioned problem, the total system performance can be significantly increased with this control approach (as shown in the next section), although the ambient conditions were much warmer, as for modes 1 and 2 (Figure 5).

4.2. Performance Assessment

The electricity consumption of the cooling tower fan and the cooling water pumps as well as the resulting *AEER* for the three presented days (Figure 5) are shown in Figure 6. It can be seen that mode 2 is not as efficient as the other two modes (*AEER* = 4.3). The main reason is a too high electricity consumption of the pump that is not justified by a gain in chiller cooling output. Mode 1 and mode 3 allow an efficient system operation with an *AEER* of 5.2 and 6, respectively. The chiller cooling power can be modulated very efficiently by adjusting the cooling water temperature. With mode 3, the efficiency can be further increased by reducing the pump power. This effect is much larger at partial load, as can be seen in Figure 7. The efficiency of mode 3 is the highest at partial load and gets closer to the efficiency of mode 1 when reaching the maximal load. Whereas the efficiency of mode 2 is high at extreme partial load, it drops dramatically when increasing the chiller capacity (due to the lack of power modulation).

More experiments than these three days have been carried out. The daily *AEER* of all measurements are plotted in Figure 8 over the daily mean wet bulb temperature T_{wb} . Since mode 2 did not show promising results, less measurement have been performed with this mode. On the contrary, mode 3 has been extensively tested. As expected, the system efficiency of each modes increases with decreasing daily average T_{wb} . Figure 8 confirms the results of the three example days presented previously. Mode 3 is the most efficient with 20% and 60% *AEER* increase compared to mode 1 and 2, respectively.

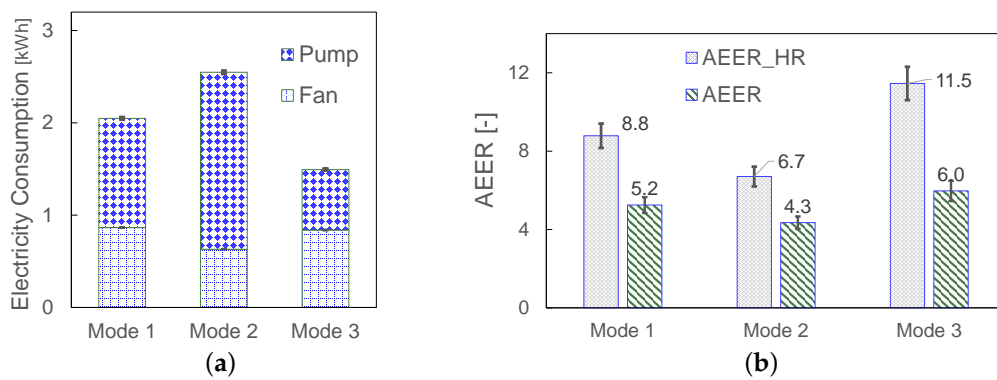


Figure 6. (a) power consumption distribution and (b) *AEER* for the three modes shown in Figure 5. The *AEER_{HR}* is the average energy efficiency ratio that considers only the measured power consumption of the heat rejection system (pump and fan).

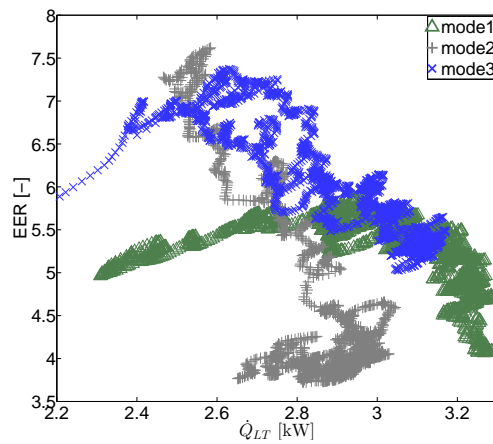


Figure 7. Energy efficiency ratios plotted against the delivered cooling capacity (for the three example days). For the sake of clarity, the *EER* values have been averaged over 5 min.

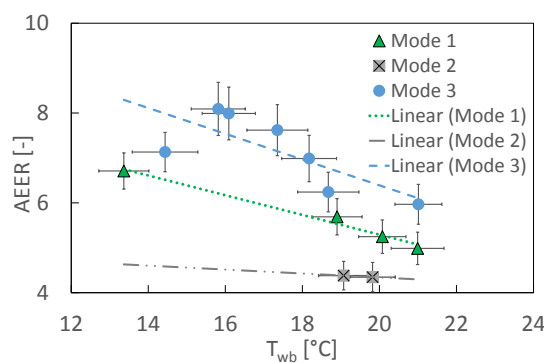


Figure 8. Daily performance of the three investigated control strategies (all measurements).

5. Conclusions

In this work, a new method for the control of solar thermally driven chillers with power modulation and optimization is proposed. It has been successfully implemented to control the cooling capacity of a diffusion absorption chiller, and the overall electrical performance has been assessed experimentally. Although this work focuses on the control of the heat rejection, the proposed method can be applied to other system parts or even to other HVAC systems as soon as the partial

load behaviour of main system parts is known (and can be characterized). The implementation of such control strategies in real systems only requires modification of the control algorithm (software) without any additional hardware costs if speed controlled pumps and fan are used. The results presented in this paper show very promising results. The implementation of such control strategies in real systems has been proven to be feasible without any particular problems. The obtained daily overall system efficiencies with the third control strategy (AEER above 6) are satisfactory despite the relatively low thermal performance of the investigated chiller [20]. Further investigations are required in order to demonstrate the reliability of such a control approach and extend its implementation in real systems. A good characterization of the main system components as well as reliable optimization algorithms are crucial for the robustness of such controls. In this regard, long-term field experiences are needed in order to test the reliability of such controls and identify further problems.

Acknowledgments: The authors acknowledge the financial support initially by the German Federal Ministry for the Environment, Nature Conservation and Nuclear Safety (BMU), and later by the Federal Ministry for Economic Affairs and Energy for the Project SolaRück (Grant number: 0325994 A). Furthermore, the authors gratefully thank the Guest Editors for the invitation to submit this paper.

Author Contributions: Antoine Dalibard elaborated on the control strategies, Antoine Dalibard conceived and designed the experiments; Antoine Dalibard, Daniel Gürlich and Dietrich Schneider performed the experiments; Antoine Dalibard and Daniel Gürlich analyzed the data; Dietrich Schneider and Antoine Dalibard modified the ammonia/water solution concentration and the chiller internal pressure to the needs of the present work; Antoine Dalibard wrote the paper with the contribution of Daniel Gürlich; and Ursula Eicker contributed to increasing the scientific level of this work.

Conflicts of Interest: The authors declare no conflict of interest.

Abbreviations

The following abbreviations are used in this manuscript:

| | |
|----------------|---|
| <i>AEER</i> | Average energy efficiency ratio |
| COP | Coefficient of performance |
| $c_{p,LT}$ | Chilled water mean specific heat ($\text{kJ} \cdot \text{kg}^{-1} \cdot \text{K}^{-1}$) |
| DACM | Diffusion absorption chilling machine |
| <i>EER</i> | Energy efficiency ratio (-) |
| f_{fan} | Fan speed frequency (Hz) |
| f_{pump} | Pump speed frequency (Hz) |
| HVAC | Heating ventilation and air conditioning |
| $P_{el,x}$ | Power consumption of pump <i>x</i> (kW) |
| $P_{el,fan}$ | Power consumption of cooling tower fan (kW) |
| $P_{el,tot}$ | Total system power consumption (kW) |
| \dot{Q}_{HT} | Chiller desorber capacity (kW) |
| \dot{Q}_{MT} | Chiller heat rejection capacity (kW) |
| \dot{Q}_{LT} | Chiller cooling capacity (kW) |
| STCS | Solar Thermally driven cooling systems |
| TDC | Thermally driven chiller |
| T_{amb} | Dry bulb or ambient temperature ($^{\circ}\text{C}$) |
| T_{wb} | Wet bulb temperature ($^{\circ}\text{C}$) |
| T_{HT} | Hot water temperature ($^{\circ}\text{C}$) |
| T_{MT} | Cooling water temperature ($^{\circ}\text{C}$) |
| T_{LT} | Chilled water temperature ($^{\circ}\text{C}$) |
| T_{set} | Chilled water temperature set point ($^{\circ}\text{C}$) |
| \dot{V}_{HT} | Hot water flow rate ($\text{m}^3 \cdot \text{s}^{-1}$) |
| \dot{V}_{MT} | Cooling water flow rate ($\text{m}^3 \cdot \text{s}^{-1}$) |
| \dot{V}_{LT} | Chilled water flow rate ($\text{m}^3 \cdot \text{s}^{-1}$) |
| ΔT_L | Temperature lift ($^{\circ}\text{C}$) |
| ΔT_L | Temperature thrust ($^{\circ}\text{C}$) |
| ρ_{LT} | Chilled water mean density ($\text{kg} \cdot \text{m}^{-3}$) |

Appendix A

The flow chart of the used optimization algorithm for one acquisition time step of mode 3 is shown in Figure A1. The variation range of the cooling water flow rate \dot{V}_{MT} is segmented in a certain number of elements. The required cooling water temperature $T_{MT,i}$ and the associated system power consumption $P_{el,tot,i}$ are calculated for each element i . The required set-points T_{MT} and \dot{V}_{MT} are determined according to the element with the minimum electricity consumption $P_{el,tot,i}$. Since the optimum has a relatively flat shape (see Figure 2), a high accuracy (i.e., a high number of elements) is not required.

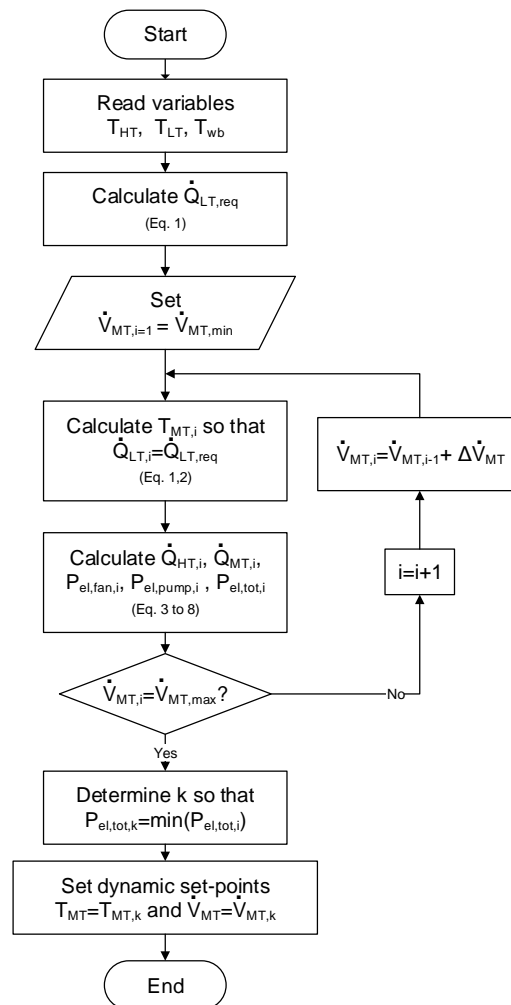


Figure A1. Flow chart of the optimization algorithm used for mode 3. In this work, the variation range of the cooling water flow rate has been segmented in 45 elements ($\dot{V}_{MT,min} = 1.8 \text{ m}^3 \cdot \text{h}^{-1}$, $\dot{V}_{MT,max} = 3.6 \text{ m}^3 \cdot \text{h}^{-1}$ and $\Delta\dot{V}_{MT} = 0.04 \text{ m}^3 \cdot \text{h}^{-1}$).

Appendix B

The derived characteristic equations of the chiller (Equations (B1) and (B2)) and the cooling tower (Equation (B3)) are based on cross correlated third-degree polynomial functions. In order to reduce the number of fitting coefficients, the chiller temperature lift $\Delta T_L = T_{MT} - T_{LT}$ and temperature thrust $\Delta T_T = T_{HT} - T_{MT}$ have been introduced. The accuracy of the obtained fits and the resulted standard deviation σ_x is shown in Figure B2:

$$\dot{Q}_{LT} = f(\Delta T_L, \Delta T_T, \dot{V}_{MT}) = \sum_{m=0}^3 \sum_{n=0}^3 \sum_{k=0}^3 C_{mnk} \cdot \Delta T_L^m \cdot \Delta T_T^n \cdot \dot{V}_{MT}^k \quad (B1)$$

$$\dot{Q}_{HT} = g(\Delta T_L, \Delta T_T, \dot{V}_{MT}) = \sum_{m=0}^3 \sum_{n=0}^3 \sum_{k=0}^3 \tilde{C}_{mnk} \cdot \Delta T_L^m \cdot \Delta T_T^n \cdot \dot{V}_{MT}^k \quad (B2)$$

$$\dot{Q}_{MT} = h(T_{CT}, T_{wb}, \dot{V}_{MT}, P_{el, fan}) = \sum_{m=0}^3 \sum_{n=0}^3 \sum_{i=0}^3 \sum_{k=0}^3 C_{mnik}^* \cdot T_{CT}^m \cdot T_{wb}^n \cdot \dot{V}_{MT}^i \cdot P_{el, fan}^k \quad (B3)$$

with $m + n + k \leq 3$ respectively, $m + n + i + k \leq 3$ and $P_{el, fan} = f(f_{fan})$

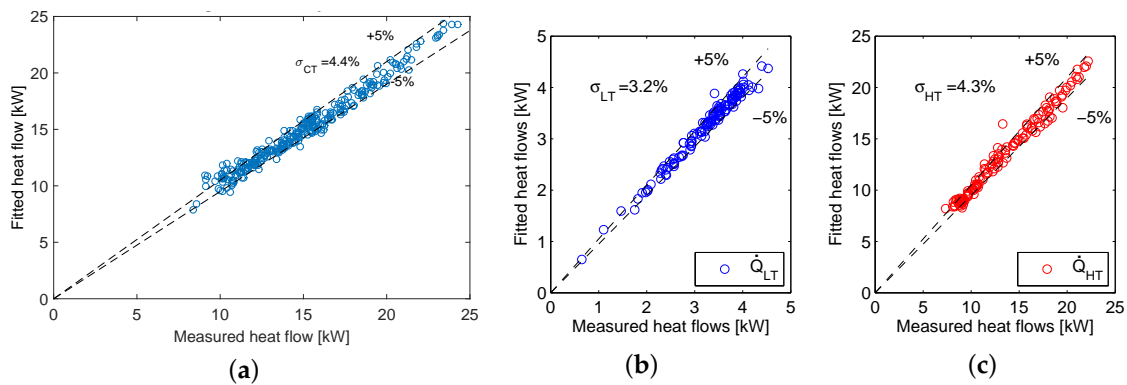


Figure B2. Fit accuracy of the characteristic equations of (a) the cooling tower \dot{Q}_{MT} ; (b) the chiller cooling capacity \dot{Q}_{LT} ; and (c) the chiller desorber capacity \dot{Q}_{HT} .

Appendix C

Figure C1 shows that the cooling load can be matched with the third control strategy if no problems occur in the starting phase. For this specific day, due to lower ambient conditions (T_{wb} around 18–19 °C), the optimized strategy was to operate the pump with low flow rate and increase the cooling tower fan speed in order to cover the load. The obtained AEEER was 6.2 ± 0.4 .

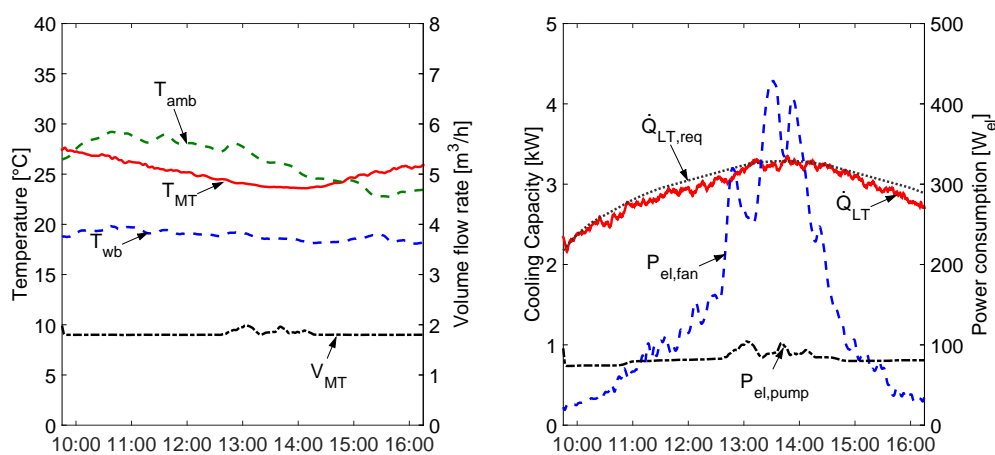


Figure C1. Another measurement sample day with matched cooling load (mode 3).

References

1. Coulomb, D.; Dupon, J.L.; Pichard, A. *The Role of Refrigeration in the Global Economy—29th Informatory Note on Refrigeration Technologies*; Technical Report; International Institute of Refrigeration: Paris, France, 2015.

2. Arent, D.J.; Tol, R.S.J.; Faust, E.; Hella, J.P.; Kumar, S.; Strzepek, K.M.; Toth, F.L.; Yan, D. *Climate Change 2014: Impacts, Adaptation, and Vulnerability. Part A: Global and Sectoral Aspects. Contribution of Working Group II to the Fifth Assessment Report of the Intergovernmental Panel of Climate Change*; Chapter Key Economic Sectors and Services; Cambridge University Press: Cambridge, UK; New York, NY, USA, 2014.
3. European Commission. *Commission Staff Working Document, Review of Available Information, Communication from the Commission to the European Parliament, the Council, the European Economic and Social Committee and the Committee of the Regions on an EU Strategy for Heating and Cooling*; SWD (2016) 24 Final, PART 1/2; European Commission: Brussels, Belgium, 2016.
4. European Commission. *Communication from the Commission to the European Parliament, the Council, the European Economic and Social Committee and the Committee of the regions. A Policy Framework for Climate and Energy in the Period from 2020 to 2030*; COM/2014/015 Final; European Commission: Brussels, Belgium, 2014.
5. Henning, H.; Döll, J. Solar Systems for Heating and Cooling of Buildings—1st International Conference on Solar Heating and Cooling for Buildings and Industry (SHC 2012). *Energy Procedia* **2012**, *30*, 633–653.
6. Calise, F. Thermoeconomic analysis and optimization of high efficiency solar heating and cooling systems for different Italian school buildings and climates. *Energy Build.* **2010**, *42*, 992–1003.
7. Reda, F.; Viot, M.; Sipilä, K.; Helm, M. Energy assessment of solar cooling thermally driven system configurations for an office building in a Nordic country. *Appl. Energy* **2016**, *166*, 27–43.
8. Jähniq, D.; Thür, A. *Monitoring Results—Technical Report of Subtask A, Pre-Engineering Systems for Residential and Small Commercial Applications*; IEA-SHC–Task38–Solar Air-Conditioning and Refrigeration; Solar Heating & Cooling Programme (SHC): Graz, Austria, 2011.
9. Kohlenbach, P. *Solar Cooling with Absorption Chillers: Control Strategies and Transient Chiller Performance*. Ph.D. Thesis, TU Berlin, Berlin, Germany, 2006.
10. Bujedo, L.; Rodríguez, J.; Martínez, P. Experimental results of different control strategies in a solar air-conditioning system at part load. *Sol. Energy* **2011**, *85*, 1302–1315.
11. Henning, H. Solar assisted air conditioning of buildings—An overview. *Appl. Therm. Eng.* **2007**, *27*, 1734–1749.
12. Lecuona, A.; Ventas, R.; Venegas, M.; Zacarías, A.; Salgado, R. Optimum hot water temperature for absorption solar cooling. *Sol. Energy* **2009**, *83*, 1806–1814.
13. Kühn, A.; Corrales Ciganda, J.; Ziegler, F. Comparison of control strategies of solar absorption chillers. In Proceedings of the 1st International Congress on Heating, Cooling and Buildings (EUROSUN 2008), Lisbon, Portugal, 7–10 October 2008.
14. Ziegler, F.; Schweigler, C.; Hellmann, H. The characteristic equation of sorption chillers. In Proceedings of the International Sorption Heat Pump Conference, Munich, Germany, 24–26 March 1999; pp. 169–172.
15. Sonntag, C.; Ding, H.; Engell, S. Supervisory Control of a Solar Air Conditioning Plant with Hybrid Dynamics. *Eur. J. Control* **2008**, *14*, 451–463.
16. Albers, J.; Kemmer, H.; Ziegler, F. Solar-driven adsorption chiller controlled by hot and cooling water temperature. In Proceedings of the 3rd International Conference Solar Air-Conditioning, Palermo, Italy, 30 September–2 October 2009.
17. Albers, J. New absorption chiller and control strategy for the solar assisted cooling system at the German federal environment agency. *Int. J. Refrig.* **2014**, *39*, 48–56.
18. Dalibard, A.; Eicker, U.; Ziegler, F. Advanced controls of solar driven adsorption chillers. In Proceedings of the 5th International Conference Solar Air-Conditioning, Bad Krozingen, Germany, 25–27 September 2013.
19. Eicker, U.; Pietruschka, D.; Pesch, R. Heat rejection and primary energy efficiency of solar driven absorption cooling systems. *Int. J. Refrig.* **2012**, *35*, 729–738.
20. Jakob, U.; Eicker, U.; Schneider, D.; Taki, A.; Cook, M. Simulation and experimental investigation into diffusion absorption cooling machines for air-conditioning applications. *Appl. Therm. Eng.* **2008**, *28*, 1138–1150.
21. Wiemken, E.; Nienborg, B.; Koch, L. Report on the methodology of the virtual case study—Solarcombiplus European Project. Fraunhofer ISE, 2009.

